Hindawi
Mathematical Problems in Engineering
Volume 2022, Article ID 2384202, 19 pages
https://doi.org/10.1155/2022/2384202

Research Article

Structure Damage Identification Based on Information Entropy and Bayesian Fusion

Chang-Sheng Xiang,[1,2] **Hai-Long Liu**,[1] **Chen-Yu Liu**,[1] **Yu Zhou**,[3] **and Li-Xian Wang**[1,2]

[1]*School of Civil Engineering, Lanzhou University of Technology, Lanzhou 730050, China*
[2]*Western Engineering Research Center of Disaster Mitigation in Civil Engineering, Ministry of Education, Lanzhou 730050, China*
[3]*College of Civil Engineering, Anhui Jianzhu University, Hefei 230601, China*

Correspondence should be addressed to Hai-Long Liu; 1220498033@qq.com

Received 25 March 2022; Accepted 6 June 2022; Published 1 July 2022

Academic Editor: Vittorio Memmolo

When processing signals, information entropy theory and data fusion theory have their own advantages. The former can improve the sensitivity of signals, while the latter can superimpose multisource information to correct system deviations and obtain the best identification results. Therefore, we introduce two theories into structural damage identification to improve the reliability of damage identification. First, based on the modal strain energy damage identification index, combined with information entropy and data fusion theory, a fusion entropy index (FE) and an entropy weight fusion index (EWF) are constructed. Then, the simply supported beam and truss structure model are established for damage simulation, which verified that the FE index and EWF index can accurately locate the damage. The polynomial fitting method is used to identify the damage degree of the structure, and the identification results obtained are more accurate. Finally, a simple-supported steel beam model is established in the laboratory for verification and analysis. The results show that the proposed FE index and EWF index have high damage sensitivity, noise resistance, and robustness, and relatively speaking, EWF index damage recognition ability is better. The method proposed in this paper provides an empirical method for practical engineering application.

1. Introduction

In the service process of bridge structure [1, 2], the material properties of structure changed, which would eventually lead to damage after long-term accumulation, and affected use function of bridge structure when reaching a certain degree. Therefore, it is necessary to identify damage location, timely evaluate damage degree, and take corresponding maintenance and reinforcement measures to ensure operation safety of structure [3].

Modal parameter is one of commonly used parameters in structure state assessment method [4, 5], based on which many damage identification indexes can be constructed [6], such as curvature mode [7, 8], frequency [9, 10], and strain energy [11, 12]. Since the curvature mode cannot be measured directly, it usually depends on the central difference calculation of vibration mode data, and its calculation error is greatly affected by data completeness and noise [13–15]. As a global variable, frequency is not sensitive to damage, and it is usually impossible to identify local damage of structures [16]. Although the identification method based on modal strain energy is also affected by completeness of mode shape, it has become one of the research hotspots because of its strong sensitivity to local damage of structures [17–20].

Information entropy, as a measure of system signal confusion, has been successfully applied to agronomy, ecology, economics, and other disciplines [21–24]. Currently, the information entropy theory in engineering field is mainly applied to mechanical failure, surrounding rock stability, dam safety, and so on, but there is little research on bridge structure damage identification. Introducing it into structural damage identification can improve damage

sensitivity and reliability of damage identification [25–27]. Bayesian data fusion is a method comprehensively considering multisource information, which possesses obvious advantages in dealing with uncertain problems. By constantly updating the prior probability, correcting the system deviation, and obtaining redundant or complementary information, the optimal solution can be obtained by fusing the redundant information [28–31]. In view of its advantages such as better fault tolerance and reliability, introducing it into the field of structural damage identification can improve the accuracy of damage diagnosis.

Based on the theory of modal strain energy and combining advantages of information entropy and Bayesian fusion theory in data processing, a damage identification method combining information entropy and Bayesian data fusion is proposed in this paper. Fusion Entropy (FE) index and Entropy Weight Fusion (EWF) index are constructed for damage localization and quantitative analysis.

2. Methodology and Index Construction

2.1. Modal Strain Energy Theory. Modal strain energy of element is a sensitive parameter in structural local damage identification. The element modal strain energy of structure is

$$MSE_{ij}^{u} = \left\{\phi_i^{\mathrm{T}}\right\}\left|K_j\right|\left\{\phi_i\right\}, \tag{1}$$

$$MSE_{ij}^{d} = \left\{\widetilde{\phi}_i^{\mathrm{T}}\right\}\left|K_j\right|\left\{\widetilde{\phi}_i\right\}, \tag{2}$$

where MSE_{ij}^{u} and MSE_{ij}^{d} are the modal strain energy of the jth element corresponding to the ith mode before and after damage respectively; K_j means the stiffness matrix of the element; ϕ_i and $\widetilde{\phi}_i$ are the mode vectors before and after structural damage. Because the stiffness K_j of the element after damage cannot be determined, the stiffness K before damage is adopted instead.

2.2. Information Entropy. The concept of entropy originated from thermodynamics [32], which is a physical quantity to express the clutter degree of molecular state. In 1948, American mathematician Shannon first proposed the concept of information entropy, which is mainly exploited to measure uncertainty of information. The formula is as follows:

$$H = -\sum_{i=1}^{m} p_i \ln\ p_i, \tag{3}$$

where H represents the amount of information; p_i indicates probability of the occurrence of the ith signal; $\ln\ p_i$ is the amount of information provided by the ith signal; m is signal length.

2.3. Bayesian Data Fusion. Bayesian data fusion is one of the most commonly used methods for multitarget information fusion decision [33]. Its principle is to constantly update prior probability according to newly measured data, so as to obtain posterior probability.

The expression of Bayesian posterior probability is

$$\begin{aligned} P(A_m \mid B) &= \frac{P(A_m B)}{P(A)} \\ &= \frac{P(B \mid A_m)P(A_m)}{\sum_{j=1}^{m} P(B \mid A_j)P(A_j)}, \end{aligned} \tag{4}$$

where $P(A_m \mid B)$ is posterior probability of the occurrence of event A_m under the condition that event B occurs; $P(A_m)$ is prior probability of event A_m; $P(B \mid A_m)$ is likelihood function of event A_m.

When the data fusion theory is applied to the research of structural damage identification, it can be expressed that if there are n information sources (or n evaluation indexes) S_1, S_2,. . .,S_n, and m independent identification targets (or m elements) A_1, A_2,. . .,A_m are to be identified, then the following conditional probability matrix is obtained for n evaluation indexes:

$$\begin{bmatrix} P(S_1 \mid A_1) & P(S_1 \mid A_2) & \cdots & P(S_1 \mid A_m) \\ P(S_2 \mid A_1) & P(S_2 \mid A_2) & \cdots & P(S_2 \mid A_m) \\ \vdots & \vdots & \vdots & \vdots \\ P(S_n \mid A_1) & P(S_n \mid A_2) & \cdots & P(S_n \mid A_m) \end{bmatrix}. \tag{5}$$

Therefore, according to Bayes theorem, the posterior probability of A_i is

$$\begin{aligned} P(A_i \mid S_1, \ldots, S_n) &= \frac{P(S \mid A_i)P(A_i)}{\sum_{j=1}^{m} P(S \mid A_j)P(A_j)} \\ &= \frac{P(S_1 \mid A_i)P(S_2 \mid A_i)\cdots P(S_n \mid A_i)P(A_i)}{\sum_{j=1}^{m} P(S_1 \mid A_j)P(S_2 \mid A_j)\cdots P(S_n \mid A_j)P(A_j)} \\ i &= 1, 2 \ldots, m. \end{aligned} \tag{6}$$

2.4. Index Construction of Damage Identification

2.4.1. Basic Indexes of Damage Evaluation

(1) As one of the basic indexes, Modal Strain Energy Change (MSEC) can be applied for damage localization [34], which is expressed as

$$MSEC_j = \frac{1}{n}\sum_{i=1}^{n} \frac{\left|C_{ij}\right|}{C_{i,\max}}, \tag{7}$$

where n is the modal order involved in calculation; C_{ij} and $C_{i,\max}$ are the strain energy increment and its maximum value, respectively, and the expression is

$$C_{ij} = SE_{ij}^{d} - SE_{ij}^{u} \cdot C_{i,\max} = \max C_{ij}. \tag{8}$$

(2) As a damage localization parameter, Modal Strain Energy Ratio Difference (MSERD) [35] can be expressed as

$$MSERD_j = \frac{1}{n}\left|\sum_{i=1}^{n} ID_{ij}\right|, \tag{9}$$

where $I\ D$ is the difference of Modal Strain Energy Ratio (MSER) before and after damage.

$$ID_{ij} = MSER_{ij}^{d} - MSER_{ij}^{u},$$
$$MSER_{ij} = \frac{MSE_{ij}}{\sum_{j=1}^{m} MSE_{ij}}. \tag{10}$$

(3) Cross-model Modal Strain Energy (CMSE) [12]:

$$CMSE_{ij}^{u} = \left\{\phi_i^{\mathrm{T}}\right\}\left|K_j\right|\left\{\phi_i\right\},$$
$$CMSE_{ij}^{d} = \left\{\phi_i^{\mathrm{T}}\right\}\left|K_j\right|\left\{\widetilde{\phi}_i\right\}. \tag{11}$$

Therefore, the Rate Change Cross-Model Modal Strain Energy (RCCMSE) can be expressed as

$$RCCMSE_j = \frac{1}{n}\sum_{i=1}^{n}\frac{CMSE_{ij}^{d} - CMSE_{ij}^{u}}{CMSE_{ij}^{u}}. \tag{12}$$

2.4.2. Construction and Normalization of Evaluation Data Matrix. Assuming that the value of the ith index of the jth identification object can be denoted as F_{ji} ($j = 1, 2, \ldots, m$; $i = 1, 2, \ldots, n$), then the evaluation data matrix is

$$F = \begin{bmatrix} F_{11} & F_{12} & \cdots & F_{1n} \\ F_{21} & F_{22} & \cdots & F_{2n} \\ \vdots & \vdots & \vdots & \vdots \\ F_{m1} & F_{m2} & \cdots & F_{mn} \end{bmatrix}. \tag{13}$$

Since there are order of magnitude differences among the evaluation index variables, it is impossible to compare them. Hence, the range standardization method is employed to normalize all the original data, which makes the processed index variables comparable. The details are as follows:

$$F'_{ji} = \frac{F_{ji} - \min F_i}{\max F_i - \min F_i}. \tag{14}$$

2.4.3. Characteristic Probability Distribution Function and Entropy. According to Equations (7), (9) and (12), each index value corresponding to the j-th element is obtained, respectively, and then the probability distribution function $P(x_{ji})$ corresponding to the j-th element in each index is calculated:

$$P\left(x_{ji}\right) = \frac{F'_{ji}}{\sum_{j=1}^{m} F'_{ji}}, \quad (i = 1, 2, 3). \tag{15}$$

Then, substituting it into equation (3), the entropy value H_{ji} can be obtained:

$$H_{ji} = -\sum_{j=1}^{m}\frac{F'_{ji}}{\sum_{j=1}^{m} F'_{ji}}\ln\frac{F'_{ji}}{\sum_{j=1}^{m} F'_{ji}}. \tag{16}$$

2.4.4. Comprehensive Entropy Q_j. If the entropy value of the ith index is H_i, the weight value of the ith index can be obtained as follows:

$$w_i = \frac{1 - \sum_{j=1}^{m} H_{ji}}{n - \sum_{i=1}^{n}\sum_{j=1}^{m} H_{ji}}, \quad \left(0 \le w \le 1, \sum_{i=1}^{t} w_i = 1\right). \tag{17}$$

In multi-index decision problems, the smaller the entropy of an index, the greater its information, the greater its role in model comprehensive evaluation, and the greater its weight.

Therefore, the comprehensive entropy Q_j of the j-th element is

$$Q_j = \sum_{i=1}^{n} w_i F'_{ji}. \tag{18}$$

2.4.5. Fusion Entropy Index FE. The fusion entropy index (FE) assumes that the prior probability of each recognized target is the same and takes average value, namely,

$$P\left(A_j\right) = \frac{1}{m} \quad \left(\sum_{j=1}^{m} P\left(A_j\right) = 1\right). \tag{19}$$

By substituting equations (16) and (19) into equation (6), so the FE index value of the j-th element is

$$FE_j = \frac{P\left(H_1, H_2, \cdots H_n | A_i\right) P\left(A_i\right)}{\sum_{j=1}^{m} P\left(H_1, H_2, \cdots H_n | A_j\right) P\left(A_j\right)}. \tag{20}$$

2.4.6. Entropy Weight Fusion Index EWF. The entropy weight fusion (EWF) means taking comprehensive entropy Q_j as the prior probability of each identification target, namely,

$$P\left(A_j\right) = \frac{Q_j}{\sum_{j=i}^{m} Q_j}. \tag{21}$$

The EWF can be constructed by substituting equations (16) and (21) into equation (6), so the index of the j-th element is calculated as follows:

$$EWF_j = P\left(A_j | H_1, H_2, \cdots H_n\right) = \frac{P\left(H_1, H_2, \cdots H_n | A_i\right) P\left(A_i\right)}{\sum_{j=1}^{m} P\left(H_1, H_2, \cdots H_n | A_j\right) P\left(A_j\right)}. \tag{22}$$

The FE index and EWF index constructed will be used to identify the structural damage and we can compare and analyze them.

3. Damage Identification of Simply Supported Beams

3.1. Finite Element Model. The model of a simply supported beam is established with ANSYS 19.2. The beam length is 6.00 m, the cross-section size is $0.20\,\text{m} \times 0.12\,\text{m}$ (width × height), the elastic modulus E is 30 GPa, Poisson's ratio $\varepsilon = 0.17$, density $\rho = 2500\,\text{kg}/m^3$, and BEAM188 is selected as the element. The whole beam structure is divided into 25 elements and 26 nodes, as shown in Figure 1.

The structural stiffness is declined by reducing element elastic modulus E, to simulate structure damage. Damage cases are established, as shown in Table 1.

3.2. Modal Analysis. Table 2 shows frequency data of the first three orders under some cases. It can be seen that, with increasing damage degree of simply supported beam, period gradually increases, and frequency gradually decreases. Figure 2 is nephogram of simply supported beams of the first three orders under nondamage case.

3.3. Damage Location Identification. Figures 3–5 demonstrate the damage location identification results of FE index and EWF index under various cases.

3.3.1. Single Damage. As shown in Figure 3, when the structure is damaged at a single point with different degrees, large peaks will occur at damage points no matter FE and EWF indexes, which can accurately determine the damage location. Comparing Figures 3(a) and 3(b), it can be found that peak values of EWF index are larger at damaged element, which indicates that it is more sensitive to damage. As damage degree goes up, the peak values of FE index and EWF index at the damage location will not change too much, implying that the peak values cannot directly reflect damage degree of structure.

3.3.2. Double Damage. Figure 4 shows that when there are two damage cases, both indexes can accurately locate damage. When damage of different degrees occurs at different locations of structure (black), peak value of the index will be large at the location with large damage degree. When damage with the same degree occurs in different locations (red), peak value near the mid-span is larger. When damage degrees of element 12 and element 18 rise to the same degree, from Case 8 to Case 9 (blue to green), peak value at damage location does not change much.

3.3.3. Multiple Damage. It can be seen from Figure 5 that when there is multiple damage, peaks appear at the damage locations, and the peak value is related to location of the damage element and the damage degree. The closer to the support, the lower the damage sensitivity, and the lower the peak value of the index, which is inconsistent with the relative value of the actual damage degree between damage elements, which further proves that there is no direct correlation between peak value and damage degree.

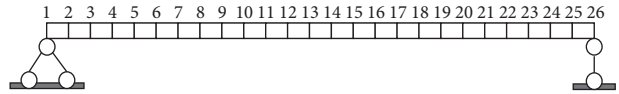

Figure 1: Model of simple-supported beam.

Table 1: Damage cases of simple-supported beam.

Damage case	Damage element no.	Damage degree %
C1~C5	6	10, 15, 20, 25, 30
C6	3, 9	15, 10
C7		15, 15
C8	12, 18	15, 20
C9		20, 25
C10		20, 25, 30
C11		25, 30, 20
C12	3, 12, 18	30, 20, 25
C13		15, 15, 15
C14		35, 35, 35

Table 2: Frequency of some cases.

Frequency	1st order mode	2nd order mode	3rd order mode
Undamaged case	5.2425	21.048	47.652
Case 1	5.2330	20.959	47.493
Case 2	5.2275	20.907	47.402
Case 3	5.2213	20.849	47.302
⋮	⋮	⋮	⋮

To sum up, both FE and EWF indexes can identify structural damage points but cannot reflect damage degree, and EWF index is more sensitive to damage.

3.4. Damage Degree Identification. In the study of structural damage degree identification, common damage degree calculation methods include the following: using crack width to express damage degree of structure [36], judging damage degree of structure by the maximum of real part of wavelet coefficient [37], calculating damage degree by sparse Bayesian algorithm [38], predicting damage degree of structure damage by BP neural network [39], and fitting damage degree identification equation by polynomial. Among them, polynomial fitting method is simple in process, easy to obtain damage degree identification curve, and high in identification accuracy. Chang-Sheng et al. [26] fitted the relationship between the proposed index and the damage degree by polynomial fitting method, to further judge the damage degree at the damage location, and the error is kept at about 10%.

This paper adopts polynomial fitting method to identify the damage degree of element under single-point damage and multipoint damage cases. By using MATLAB to calculate the peak value of FE index and EWF index at the damage location, and combining with corresponding relationship between actual damage degree, polynomial fitting

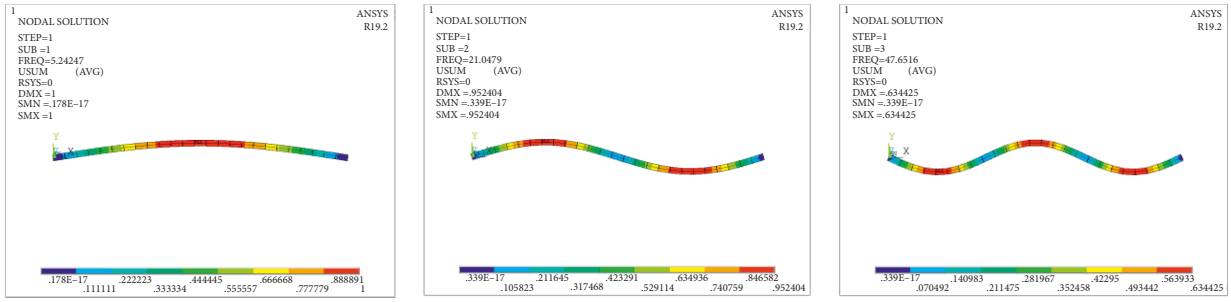

(a) (b) (c)

Figure 2: Modal shape cloud diagram of nondamage case.

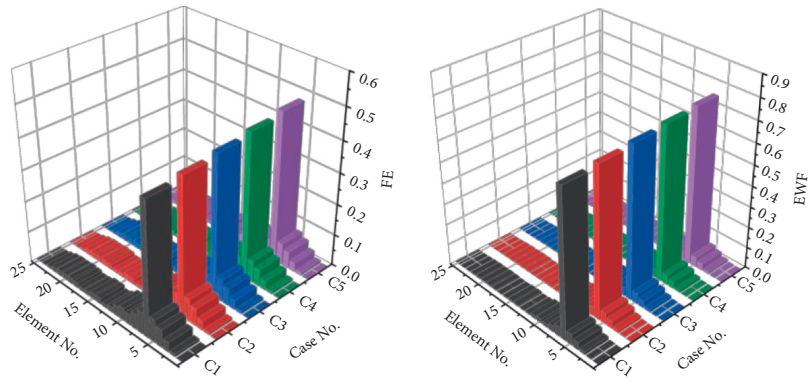

(a) (b)

Figure 3: Single damage recognition result. (a) FE. (b) EWF.

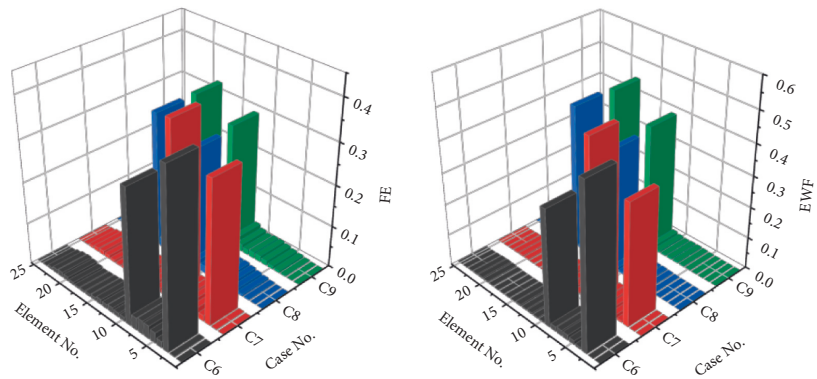

(a) (b)

Figure 4: Two damage identification results. (a) FE. (b) EWF.

method is used to fit the damage degree identification curves in MATLAB, respectively.

The damage degree is calculated with the fitted polynomial and is compared with the actual damage degree. Sum of squared error (SSE) and determination coefficient (R^2) are used as the evaluation criteria of fitting curve accuracy. The smaller the SSE, the stronger the correlation between fitting data and fitting function. The closer R^2 is to 1, the better the fitting effect is. The normal range of R^2 is [0, 1].

$$R^2 = \frac{\sum_{i=1}^{n} (y_i - \overline{y})^2 - \sum_{i=1}^{n} (\widehat{y}_i - \overline{y})^2}{\sum_{i=1}^{n} (y_i - \overline{y})^2}, \tag{23}$$

where y is the true value, $\overline{y}$ is the average value, and $\widehat{y}$ is the estimated value.

3.4.1. Single Damage. Cases 1~5, respectively, represent different damage cases of Element 6. The peak values of FE index and EWF index of Element 6 under each case are

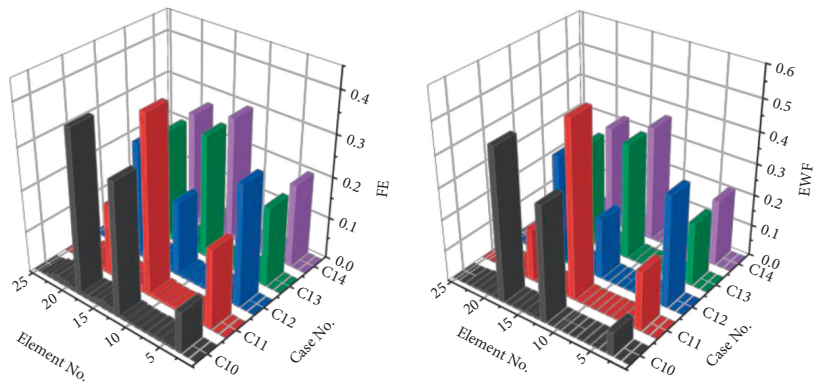

(a) (b)

Figure 5: Multiple damage identification results. (a) FE. (b) EWF.

obtained by calculation (seen Table 3). According to the corresponding relationship between peak value and damage degree in Table 3, two relationship curves are fitted, corresponding to two polynomials $y(x_F)$ and $y(x_E)$, and the degree of polynomial is 3. The expression is as follows:

$$y(x_F) = 2.968e-04x^3 - 1.523e-04x^2 + 6.584e-05x + 3.734e-05, \quad (24)$$

$$y(x_E) = 1.702e-05x^3 - 7.567e-06x^2 + 5.379e-06x + 4.224e-06. \quad (25)$$

Sum of squares of errors SSE and determination coefficient R^2:

$$SSE_F = 1.622e-15 R_F^2 = 0.992, \quad SSE_E = 4.737e-18 R_E^2 = 0.998. \quad (26)$$

From R^2, it can be seen that the R^2 of FE index and EWF index is greater than 0.8, and the fitting effect is good. From SSE, it can be seen that the SSE value of EWF index is smaller, so the fitting effect of EWF index is better theoretically.

When the damage of Element 6 is 22%, 35%, and 40%, the peak values of FE index and EWF index are brought into their respective fitting functions for validity verification and comparative analysis, and the results are shown in Table 4. Among them, the effectiveness evaluation index adopts relative percentage error RPE.

$$RPE = \frac{|y_i - \hat{y}_i|}{y_i} \times 100\%. \quad (27)$$

It can be seen from Table 4 that the identification errors of damage degree obtained by fitting function of FE index and EWF index are less than 5%, which shows that the two fitting functions (24) and (25) are effective, and the RPE of EWF fitting function is smaller, and the fitting damage degree is closer to real damage degree, and the fitting effect is better, which is consistent with theoretical analysis results.

Figure 6 shows the fitting curve of structural damage degree, only considering damage less than 50%, and the FE and EWF fitting curves approximate linear growth pattern in the range of 0~20% damage degree, which indicates that the structural damage is in the initial development stage. When damage degree is greater than 20%, slope of fitting curve increases rapidly, damage degree and fitting value change nonlinearly, and the structure is in the elastic-plastic change stage.

Table 3: Peaks of FE and EWF of single damage.

Damage element	Damage degree %	FE (e-05)	EWF (e-06)
6	10	4.26915	4.70279
	15	4.48086	4.91890
	20	4.67598	5.13157
	25	4.89362	5.36267
	30	5.13919	5.61586

3.4.2. Multiple Damage. When multiple damage occurs in the structure, the calculation cases of damage degree are shown in Table 5. The peak values of FE index and EWF index of damage location are shown in Table 6. According to the corresponding relationship between damage degree and peak value in Table 6, three relationship curves are fitted for each of two indexes, as shown in equations (27)~(32).

The SSE of EWF index is smaller in the fitting curve of each element under multipoint damage, meaning that the fitting effect is better.

The peak values of FE index and EWF index in cases 17, 19, and 22 are compared with the damage degree obtained by polynomial fitting, and the results are shown in Table 7. The damage degree RPE calculated by polynomial fitting is less than 1%, and the RPE of EWF index is smaller in most cases, implying that the fitting equation of damage degree is also effective and highly accurate under multiple damage cases.

(1) Fitting function of element 3:

$$y(x_{F3}) = 2.268e-06x^3 + 1.584e-05x^2 + 4.382e-06x + 2.549e-05, \quad (28)$$

$$y(x_{E3}) = 7.163e-07x3 + 1.319e-06x2 + 4.406e-07x + 1.967e-06. \quad (29)$$

$$\mathrm{SSE}_{F3} = 2.599e-14 \; R_{F3}^2 = 0.991$$

Table 4: Validation of single damage fitting function.

Damage element no.	Damage degree %	FE (*e*-05)	EWF (*e*-06)	y_F (*e*-05)	y_E (*e*-06)	RPE (FE) %	RPE (EWF) %
6	22	4.75	5.22	4.7614	5.2224	0.24	0.05
	35	5.41	5.89	5.4453	5.9094	0.65	0.32
	40	5.70	6.18	5.8303	6.2542	2.23	1.19

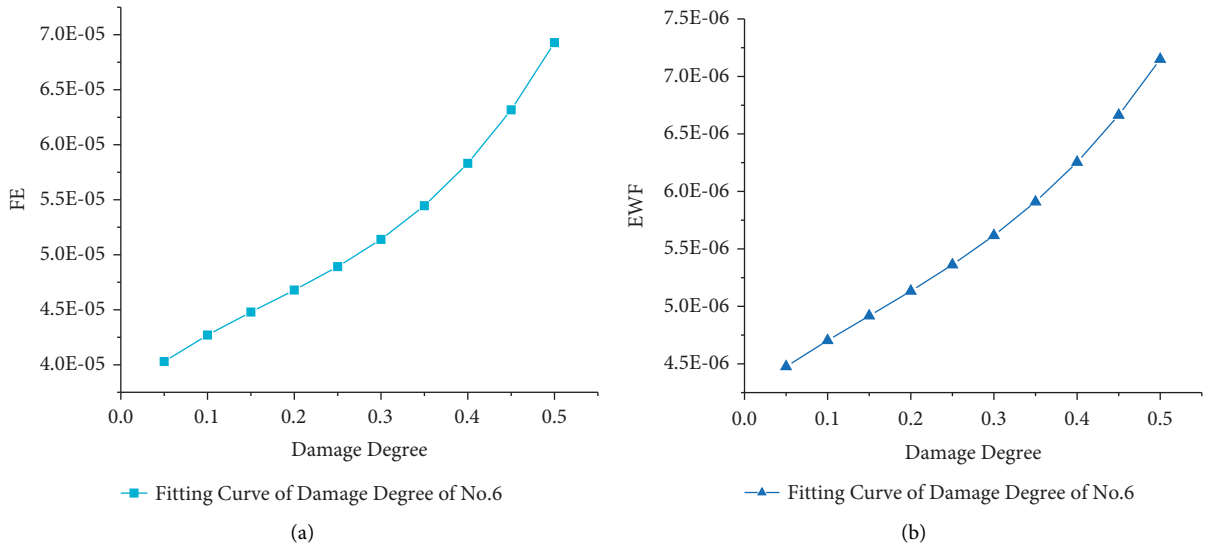

Figure 6: Fitting curve of single damage degree of simply supported beam.

Table 5: Multiple damage fitting conditions.

Damage case	Damage element no.	Damage degree %
C15~C20	3, 12, 18	5, 5, 5 10, 10, 10 13, 13, 13 20, 20, 20 22, 22, 22 25, 25, 25
C21~C25	3, 12, 18	30, 30, 30 38, 38, 38 40, 40, 40 45, 45, 45 50, 50, 50

Table 6: Peak values of FE and EWF for multiple damage.

Damage element No.	0.05		0.1		0.20		0.25		0.30		0.40		0.45		0.50	
	FE	EWF	FE	EWF	FE	EWF	FE	EWF	FE	EWF	FE	EWF	FE	EWF	FE	EWF
3	2.58	2.00	2.60	2.01	2.70	2.11	2.76	2.17	2.83	2.24	2.99	2.40	3.09	2.50	3.20	2.61
12	4.05	3.75	4.05	3.75	4.15	3.85	4.20	3.90	4.26	3.97	4.39	4.11	4.46	4.19	4.55	4.28
18	3.63	3.21	3.62	3.20	3.73	3.32	3.78	3.37	3.85	3.44	3.98	3.58	4.07	3.68	4.16	3.78

$$\mathrm{SSE}_{E3} = 2.253e-16 \quad R^2_{E3} = 0.994$$

(2) Fitting function of element 12:

$$y(x_{F12}) = -1.69e-05x^3 + 2.698e-05x^2 + 8.905e-07x + 4.034e-05, \tag{30}$$

$$y(x_{E12}) = -1.373e-06x^3 + 2.564e-06x^2 + 1.679e-07x + 3.72e-06. \tag{31}$$

$$\mathrm{SSE}_{F12} = 6.113e-14 \quad R^2_{F12} = 0.997$$
$$\mathrm{SSE}_{E12} = 5.403e-16 \quad R^2_{E12} = 0.998$$

(3) Fitting function of element 18

$$y(x_{F18}) = -1.099e-05x^3 + 2.371e-05x^2 + 2.031e-06x + 3.599e-05, \tag{32}$$

$$y(x_{E18}) = -6.807e-07x^3 + 2.195e-06x^2 + 2.635e-07x + 3.18e-06. \tag{33}$$

$$\mathrm{SSE}_{F18} = 6.744e-14 \quad R^2_{F18} = 0.996$$
$$\mathrm{SSE}_{E18} = 6.242e-16 \quad R^2_{E18} = 0.998.$$

The fitting curve of damage degree is shown in Figure 7. Comparative analysis shows that change trend of three fitting curves in two charts is similar. Before 15% damage, the three curves all change linearly, when damage degree is 15%~20%, slopes of curves begin to increase gradually, and when damage degree is greater than 20%, slope of three fitting curves increases obviously, which is consistent with change trend of FE and EWF index peaks in Table 6. Comparing the fitting curves of different elements in the figure, it can be seen that, under the same damage degree, the function curve of Element 12 near the mid-span is at the top, followed by Element 18 near 3/4 location, and the function curve of Element 3 near 1/8 location at the bottom, indicating that, under the same damage, the closer to the mid-span, the greater the values of FE index and EWF index. It can be seen from Figure 7 that the relative size of damage degree at different locations cannot be directly compared from ordinate value of the graph.

3.5. Noise Immunity Analysis. Ambient noise often exists in the measured signals [40]. Noise will exert a great impact on the identification ability and accuracy of indexes, so it is particularly important to analyze the antinoise performance of indexes in structural damage identification.

Currently, there are two methods to add noise in antinoise analysis [41]: one is to add noise to the simulated vibration signal and express noise level by signal-to-noise ratio; the other is to add noise to modal parameters obtained during modal analysis. The indexes FE and EWF proposed in this paper are calculated from modal parameters, so the noise is added to modal parameters.

Noise is added as follows:

$$\phi^n_{ij} = \phi_{ij} + \phi_{\max,i} \times randn \times \delta, \tag{34}$$

where ϕ_{ij} and ϕ^n_{ij} represent mode vectors before and after noise addition; $\phi_{\max,i}$ is the maximum value of the ith order mode shape; *randn* represents Gaussian white noise with mean value and standard deviation of 0 and 1, respectively; δ represents the noise level in the mode.

In this paper, the index antinoise ability is mainly considered when there is multiple damage, so cases 10~12 are selected for index antinoise analysis, and 0.1 and 0.15 are taken for δ to indicate that 10% and 15% noise levels are added. The identification results are shown in Figures 8 and 9.

It can be seen from Figures 8 and 9 that the peaks of FE index and EWF index are obvious at damage points, which can be accurately searched. With noise level rises, the peak value of damage point is still relatively large, which shows that FE index and EWF index have strong antinoise ability. Compared with (a) and (b), the peak value of EWF index is higher at the damaged location and the curve of undamaged location is smoother, which means that the EWF index has stronger antinoise ability and better robustness.

4. Damage Identification of Truss Structure

4.1. Finite Element Model. It is known that the damage identification method combining information entropy and data fusion has been well applied in simply supported beam bridge model, but feasibility of this method has yet to be verified for complex structure. Therefore, this paper selects truss structure as the research object to verify effectiveness of the proposed method.

A steel truss structure model is constructed by finite element software, which is composed of upper chord, lower chord, and web member, as shown in Figure 10. The whole structure is divided into six sections, each with a width of 10 meters and a height of 16 meters. The bar materials are I-beam with a specification of $0.4 \times 0.4 \times 0.016 \times 0.016$. The elastic modulus E of I-beam is 210 GPa, Poisson's ratio $\varepsilon = 0.3$, and density $\rho = 7850$ kg/m3. There are 54 beams in the whole structure, so it is divided into 54 elements. BEAM188 model is adopted, and the constraint form is shown in Figure 10, with one end being fixed constraint and the other end being sliding constraint.

The damage of truss is mainly divided into upper chord damage, lower chord damage, and web member damage. Thus, damage cases shown in Table 8 are established, and the number of each member is shown in Figure 10(b). Figure 11 is the nephogram of the first three modes of truss structure in healthy state.

4.2. Damage Location Identification

4.2.1. Identification Results of Upper and Lower Chords. The upper chord identification results are shown in Figure 12, and the damage case is set at Element 45. It can be seen from the figure that FE index and EWF index both show peak value in Element 45, which can locate the damage. However, locations of some healthy elements will also

Table 7: Validation of multiple damage fitting functions.

Damage degree %	Damage element	FE (*e*-05)	EWF (*e*-06)	YF (*e*-05)	YE (*e*-06)	RPE (FF) %	RPE (EWF) %
13	3	2.6342	2.0483	2.6332	2.0481	0.04	0.01
	12	4.0809	3.7859	4.0875	3.7821	0.16	0.10
	18	3.6665	3.2500	3.6631	3.2499	0.09	0.01
22	3	2.7254	2.1357	2.7245	2.1354	0.03	0.01
	12	4.1692	3.8713	4.1662	3.8664	0.07	0.13
	18	3.7499	3.3368	3.7467	3.3370	0.08	0.01
38	3	2.9661	2.3700	2.9567	2.3642	0.32	0.25
	12	4.3628	4.0788	4.3647	4.0787	0.19	0.01
	18	3.9672	3.5556	3.9583	3.5597	0.22	0.11

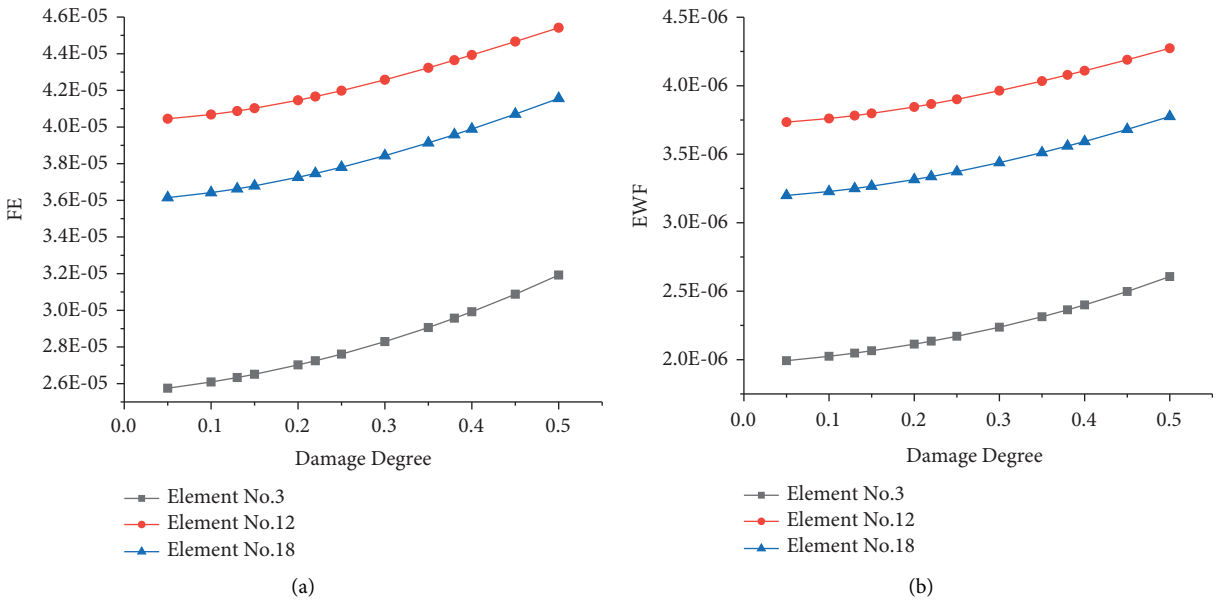

Figure 7: Fitting curve of multiple damage levels.

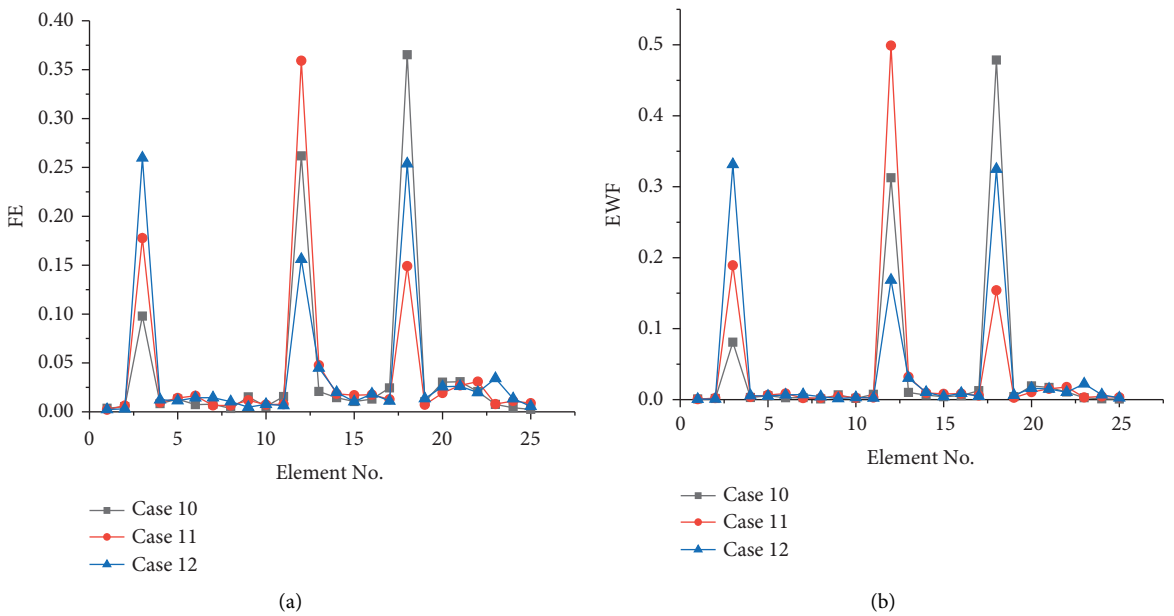

Figure 8: 10% noise level indicator recognition results.

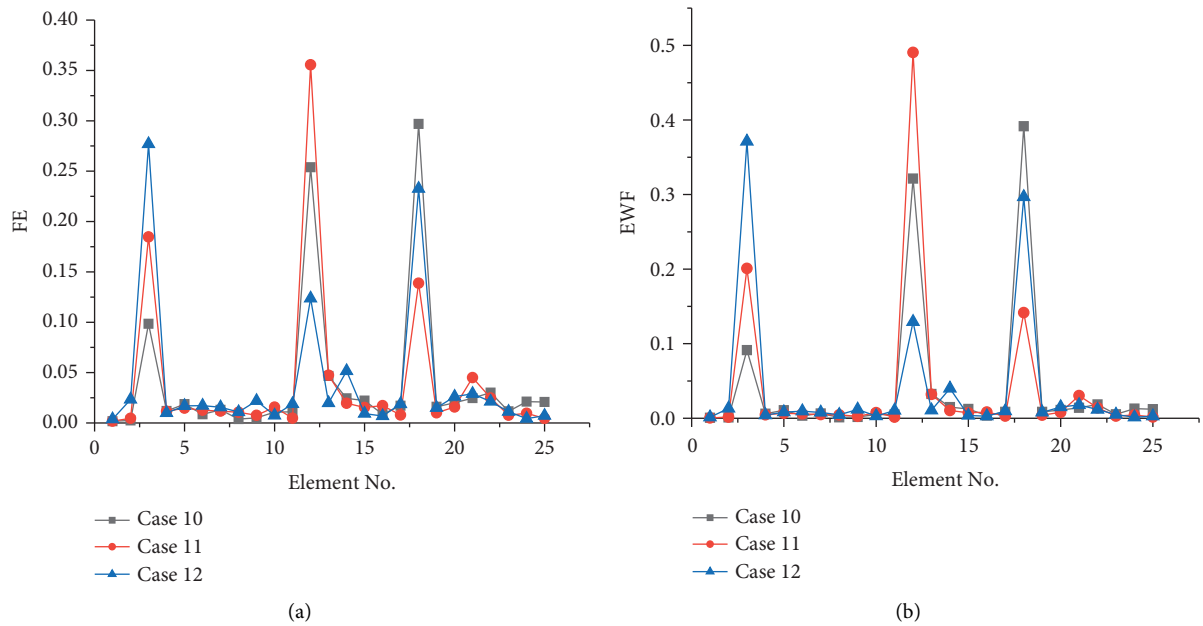

Figure 9: 15% noise level indicator recognition results.

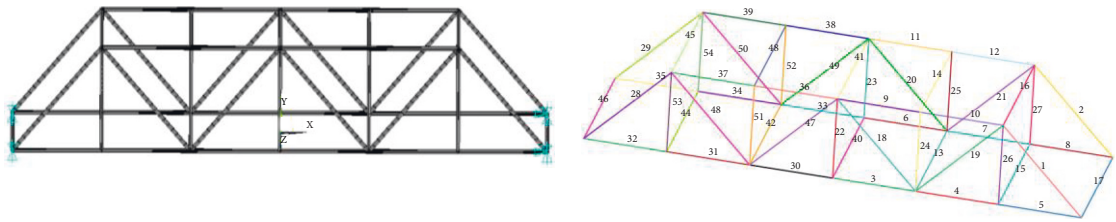

Figure 10: Finite element model of truss structure.

Table 8: Damage cases of truss structure.

Damage case	Damage element no.	Damage Degree (%)
C26–C32	45 (upper chord)	5, 10, 15, 20, 25, 30, 35
C33–C38	4 (lower chord)	5, 10, 20, 25, 30, 35
C39–C41	47 (web member)	15, 25, 30

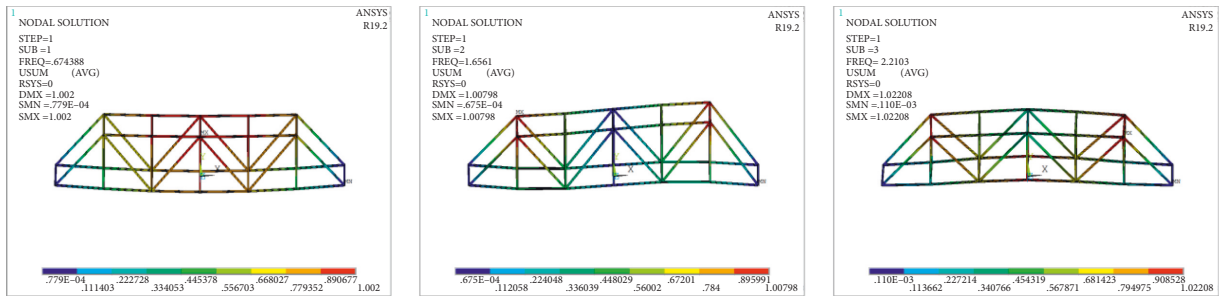

Figure 11: Mode cloud diagram of truss structure in nondestructive case.

change suddenly, such as Element 48 and Element 50. The analysis shows that this is because Element 48 and Element 50 are in the same node with the damaged element, and the damaged element will have an impact on health elements in the same node through connection between the nodes, and the impact will change with location. Compared with

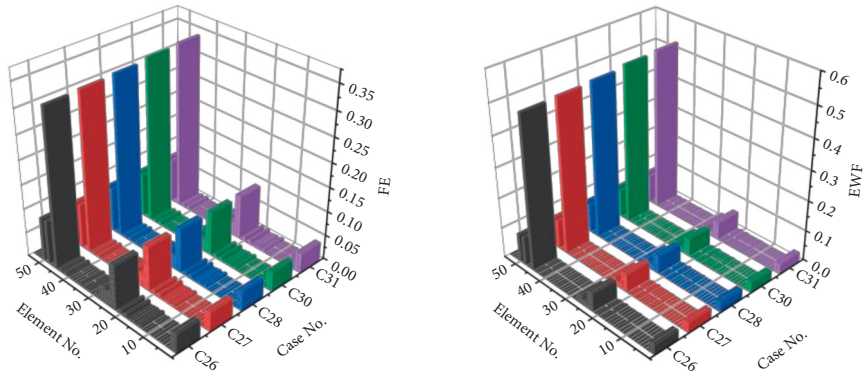

(a) (b)

Figure 12: Recognition result of upper chord.

Figures 12(a) and 12(b), it can be seen that the peak value of EWF index at damage location is larger, and the interference in health elements is smaller, so the damage localization result is more reliable.

Figure 13 demonstrates identification results of the lower chord, and the damage of Element 4 is set. It can be seen from the figure that both FE index and EWF index have large peaks at damage location, and the mutation degree of the joint element with Element 4 and other health elements is small, which can accurately identify the damage position, and the damage localization accuracy of EWF index is higher.

Compared with Figures 12 and 13, it can be seen that damage of the upper chord has a greater impact on the whole structure than damage of the lower chord. With improvement of damage degree, values of EWF index and FE index will not change too much.

4.2.2. Web Member Identification Results. Figure 14 shows identification results of web member, and the damage location is at Element 47. It can be seen from the figure that there are peaks in both indexes at damaged position, and peak value of EWF index is larger. However, because there are as many as 10 rods at the same node with Element 47, including upper and lower chords and web member, there will be more mutations at undamaged points, and the degree of mutations varies with different locations. As damage degree increases, the degree and probability of mutation of health elements increase, and elements show irregular changes, which easily interfere with judgment of damage position and can not accurately distinguish the damaged elements but can only be estimated by the relative size of ordinate values.

To sum up, FE index and EWF index can play a better role in damage localization when the upper chord and lower chord of truss structure are damaged. However, in damage identification of web members, its damage localization ability is poor.

4.3. Damage Degree Identification

4.3.1. Identification of Upper Chord Damage Degree. When the upper chord of truss structure is damaged, such as cases C26~C32, the peak value of FE index and EWF index corresponding to each condition is shown in Table 9. According to the corresponding relationship between the peak value and the damage degree, two polynomials are fitted, and the degree of polynomials is 3, and the damage degree function of No. 45 upper chord can be obtained, as shown in formulae (35) and (36):

$$y(x_F) = -4.158e-05x^3 + 5.302e-05x^2 + 5.979e06x + 4.281e-05, \quad (35)$$

$$y(x_E) = -3.234e-06x^3 + 4.8e-06x^2 + 6.819e-07x + 3.254e-06. \quad (36)$$

Sum of squared errors:

$$SSE_F = 2.03e-17 SSE_E = 5.721e-20. \quad (37)$$

When the damage of No.48 rod is 20% and 35%, the peak values of FE index and EWF index are taken to verify the effectiveness of equations (35) and (36), and the results are shown in Table 10.

It can be seen from Table 10 that the fitting results of the two indexes are close to the calculation results, and the RPE is very small and can be ignored, indicating that the two fitting polynomials are effective and reliable.

The fitting curve of upper chord damage degree is shown in Figure 15. It can be seen that as the damage degree improves, the FE value and EWF value of damage element also rise. When the damage degree is greater than 10%, the slope of the two curves changes obviously, and the damage curve increases nonlinearly, indicating that the upper chord may enter the stage of instability development at this time.

4.3.2. Identification of Lower Chord Damage Degree. When the lower chord is damaged, the peak value of FE index and EWF index corresponding to each case is shown in Table 11. According to the relationship between the damage degree and the peak value, two curves corresponding to two polynomials are obtained, as shown in equations (38) and (39):

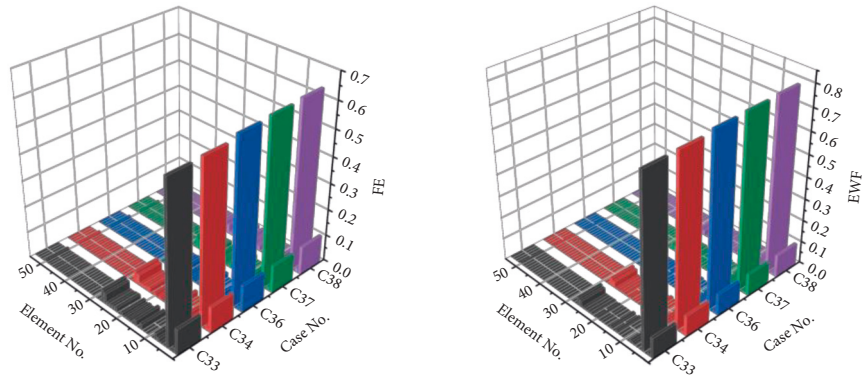

Figure 13: Recognition result of lower chord.

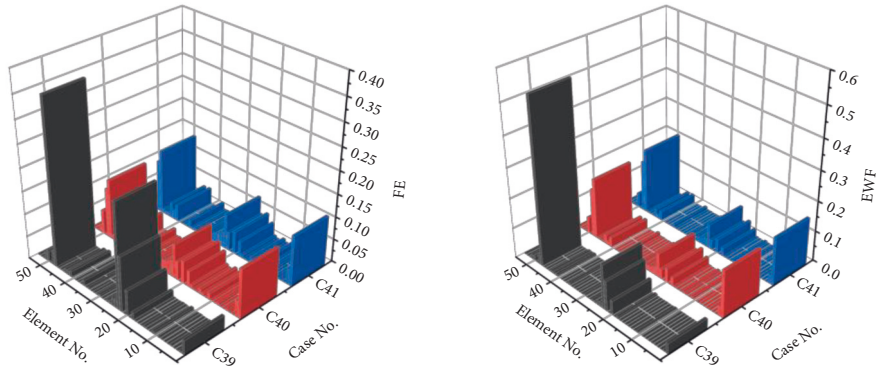

Figure 14: Results of web rod recognition.

Table 9: FE value and EWF value of different damage of upper chord.

Damage element	Damage degree%	FE (*e*-05)	EWF (*e*-06)
48	5	3.06006	2.13162
	10	3.07368	2.14795
	15	3.09163	2.16822
	25	3.13355	2.21615
	30	3.15751	2.24344

Table 10: Verification of the validity of the upper chord damage fitting function.

Damage element	Damage degree %	Indexes	Calculated value	Fitted value	RPE %
48	20	FE (*e*-05)	3.11136	3.11149	0.004
		EWF (*e*-06)	2.19089	2.19097	0.003
	35	FE (*e*-05)	3.18377	3.18214	0.051
		EWF (e-06)	2.27327	2.27201	0.056

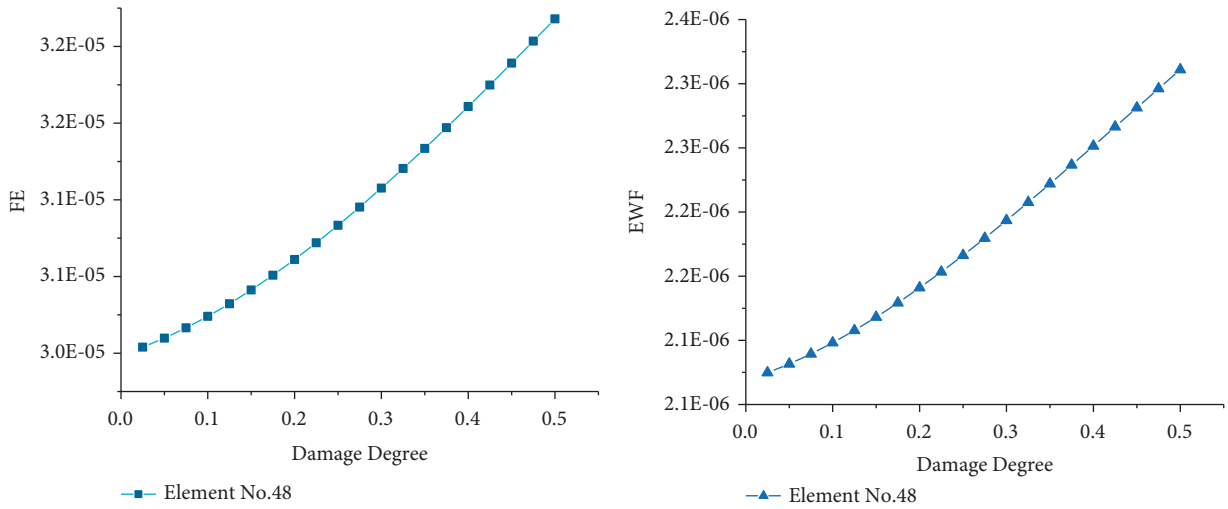

Figure 15: Fitting curve of upper chord damage degree.

Table 11: FE value and EWF value of different damage of lower chord.

Damage element	Damage degree %	FE (*e*-05)	EWF (*e*-06)
4	5	4.32419	3.30033
	10	4.38968	3.36715
	25	4.69815	3.67517
	30	4.82460	3.80285
	35	4.96222	3.84279

$$y(x_F) = -4.158e-05x^3 + 5.302e-05x^2 + 5.979e06x + 4.281e-05, \quad (38)$$

$$y(x_E) = -3.234e-06x^3 + 4.8e-06x^2 + 6.819e-07x + 3.254e-06. \quad (39)$$

Sum of squared errors:

$$SSE_F = 2.03e-17 SSE_E = 1.533e-18. \quad (40)$$

When the damage of Element 4 is 20%, the calculated values and fitting values of FE index and EWF index are taken to verify the effectiveness of equations (38) and (39), and the results are shown in Table 12.

It can be seen from Table 12 that the RPE of the two fitting polynomials is equal and kept within 1%, implying that the fitting polynomial is effective. Compared with the fitting function of the upper chord, the RPE of the lower chord increases obviously when the polynomial takes the same degree.

The fitting curve of the damage degree of lower chord is shown in Figure 16. It can be seen from the figure that, with the increase of damage degree, FE value and EWF value also increase. Compared with Figure 15, it is found that the change trend of damage degree curve of lower chord is close to that of the upper chord.

4.4. Noise Immunity Analysis. It is known that FE index and EWF index have better identification ability in damage identification of upper chord and lower chord of truss structure. Then, 10% and 15% noises are added to the vibration mode data obtained by simulation of upper chord and lower chord, respectively, to analyze the antinoise performance.

The noise addition mode is the same as that of the simply supported beam. Three conditions of upper chord in Table 8 are selected for analysis, and the identification results are shown in Figures 17 and 18.

4.4.1. Identification Results of Upper Chord. Figure 17 shows the upper chord identification results. It can be seen from figures (a) and (b) that when the noise level is 10%, FE index and EWF index will peak at the damage location, and the greater the damage degree, the greater the peak. The smaller the damage degree, the smaller the peak value, the greater the mutation probability of health elements, and the greater the interference to the judgment of damage location, as shown in the C27 identification curve (black) in the figure, which is prone to misjudgment.

When noise level increases to 15%, as shown in figures (c) and (d), the number and degree of mutation in health elements increase, and the peak value of damage position

Table 12: Validity verification of damage fitting function of lower chord.

Damage element	Damage degree %	Indexes	Calculated value	Fitted value	RPE %
4	20	FE (*e*-05)	4.58659	4.57940	0.16
		EWF(*e*-06)	3.56229	3.55651	0.16

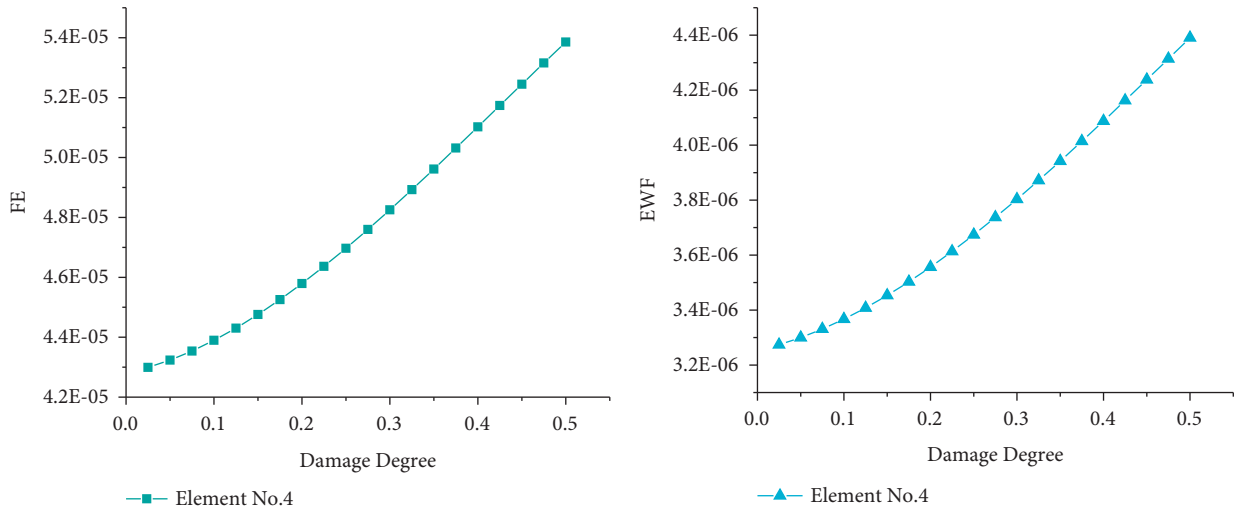

Figure 16: Fitting curve of damage degree of lower chord.

decreases. For minor damage, such as C27, both FE index and EWF index fail to identify the damage position.

Comparing identification results of two indexes, it can be seen that the peak value of EWF index is larger, damage probability of health elements is smaller, and antinoise ability is better.

4.4.2. Identification Results of Lower Chord. Figure 18 demonstrates the damage identification results of lower chord. When the noise level is 10%, the damage location can be identified by FE and EWF indexes, and the interference of health elements is small. With the increase of noise level to 15%, the probability of mutation of health elements increases, and when damage is small (black curve), both indexes are prone to misjudgment. It can be seen from the figure that the identification ability of EWF is still better in damage identification of lower chord.

Compared with Figures 17 and 18, it can be seen that the antinoise performance of FE index and EWF index is different when the damage degree of upper and lower chords is the same, and the damage location of lower chords is easier to identify.

5. Experimental Verification

5.1. Experiment Overview. In order to further verify effectiveness of two indexes, a simply supported beam test is conducted for verification and analysis, which is shown in Figure 19. The test model is a rectangular steel plate beam, section size is 100 mm × 8 mm (width × height), beam length is 2000 mm, the calculated span is 1750 mm, the elastic modulus is $E = 2.0795 \times 10^8\ \mathrm{kN/m^2}$ and the density of material $\rho = 7698\ \mathrm{kg/m^3}$.

The simply supported steel beam is divided into 35 elements and 36 joints within the calculated span length range. Acceleration sensors are installed at the nodes of elements to obtain acceleration information of structure. The experiment is carried out by single-point excitation and multipoint acceleration acquisition. The information acquisition system is INV-9812, and the signal analysis system is DASP2003.

Six signal sensors are selected to obtain the acceleration signal of structure, among which five sensors are set as a working group, distance between sensors is 5 cm, and remaining sensor serves as a control group. Based on control group, the relative value of working group data is calculated. The data collected on-site is shown in Figure 20.

5.2. Damage Simulation and Parameter Acquisition. The damage simulation in this test is realized by cutting the steel beam symmetrically. The damage conditions and actual notch forms of the steel beam are shown in Figure 21, the cutting width is 10 *mm*, and the damage location is shown in Table 13.

The stochastic subspace method is adopted to calculate modal frequency and mode shape data of structure. The obtained acceleration-time curve is processed by fast Fourier transform, and the corresponding spectrum curve of each condition is obtained, as shown in Figure 22.

5.3. Damage Location Identification. The modal data of the first three orders of structure measured by the test are processed, and the FE index and EWF index values under

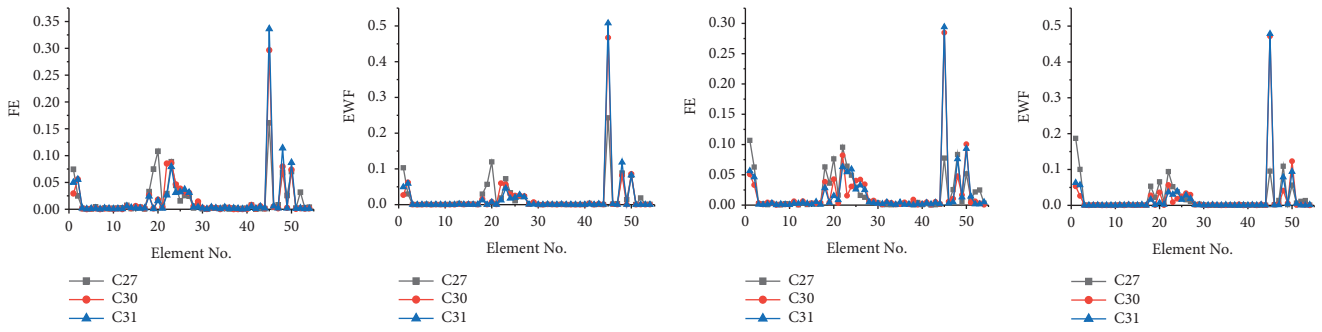

Figure 17: Recognition result of upper chord.

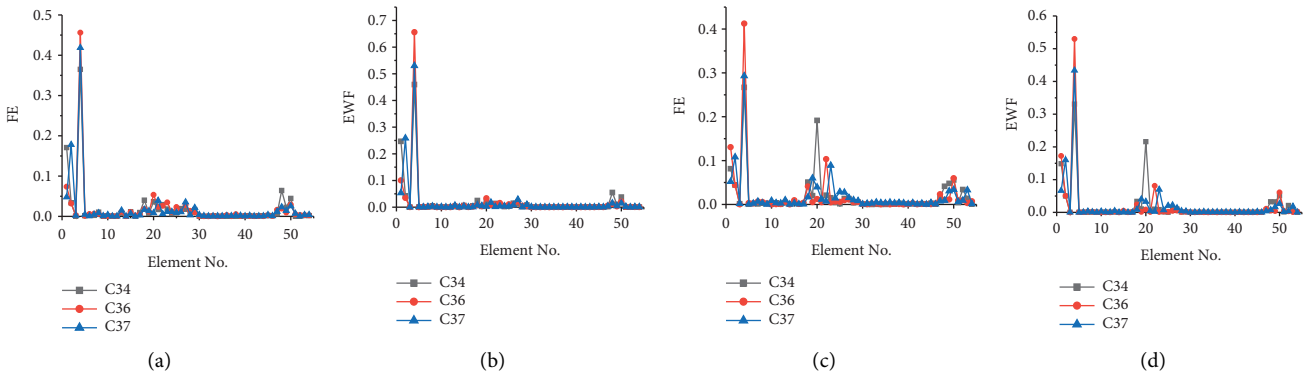

Figure 18: Recognition result of lower chord.

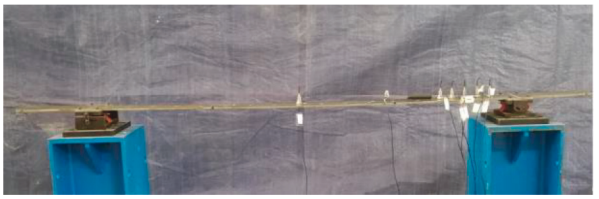

Figure 19: Laboratory simply supported steel beam model.

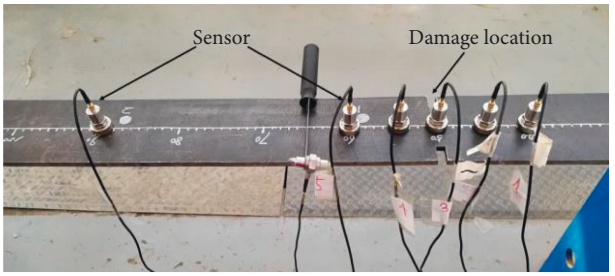

Figure 20: Data acquisition of simply supported beam.

each damage case are calculated by MATLAB software programming for damage identification analysis. The identification results are shown in Figure 23.

It can be seen from Figure 23 that although the test process will be affected by environmental noise, measurement error, human operation, and other factors, resulting in deviation of the measured vibration mode data of structure, FE index and EWF index can still accurately identify the damage location of simply supported beams.

It can be seen from Figure (a) that when the single-point damage of the test beam occurs, both the FE index and the EWF index show peaks at damaged position, and the peak

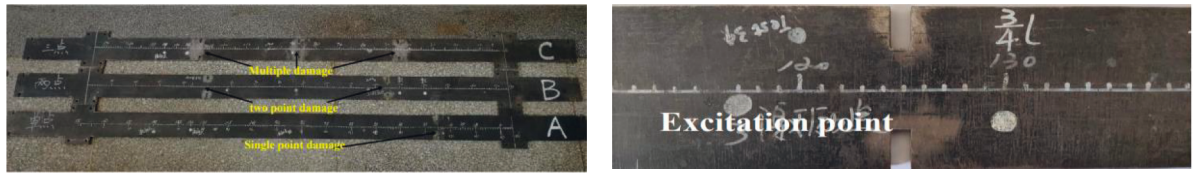

(a) (b)

Figure 21: Damage form of steel beam. (a) Steel beam damage case. (b) Steel beam notch form.

Table 13: Damage condition of steel beam test.

Damage form	Damage position and cutting depth	Damage degree %
1	No damage	
2	300 mm cut 25 mm	50
3	500 mm cut 20 mm	40
	1250 mm cut 25 mm	50
4	450 mm cut 20 mm	40
	875 mm cut 20 mm	40
	1300 mm cut 20 mm	40

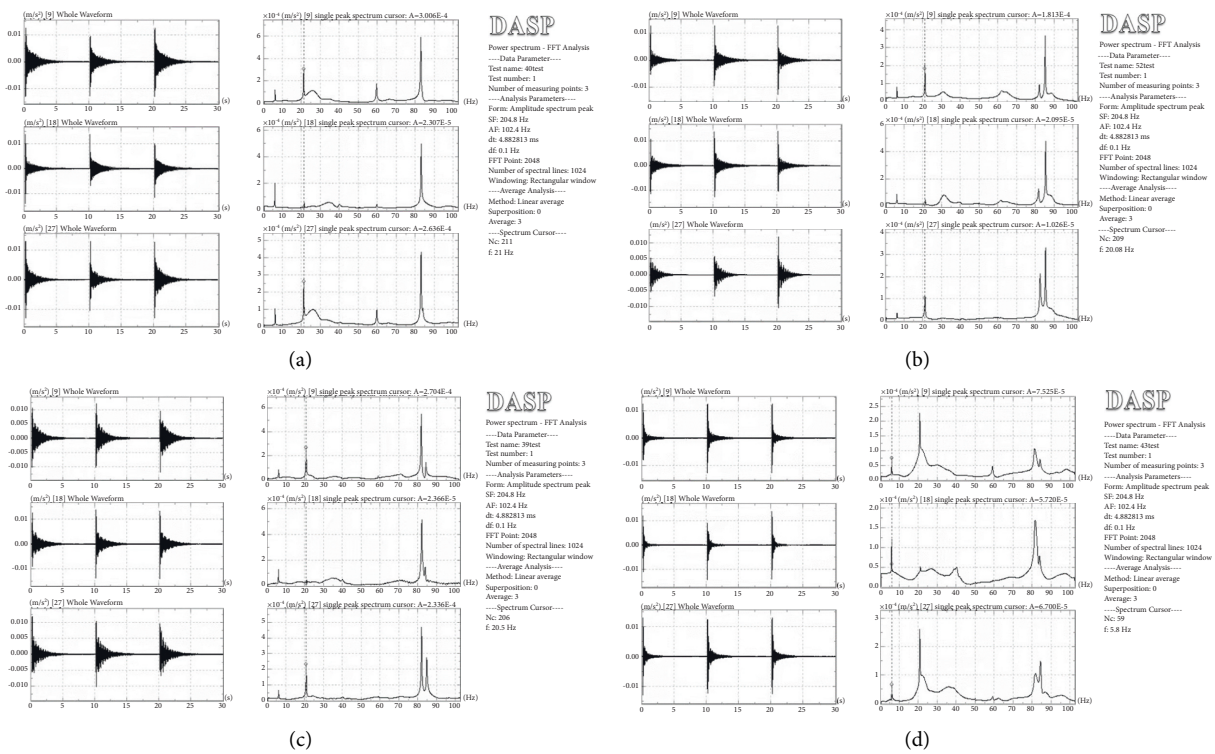

(a) (b) (c) (d)

Figure 22: Frequency spectrum curve of simply supported beam. (a) Form 1. (b) Form 2. (c) Form 3. (d) Form 4.

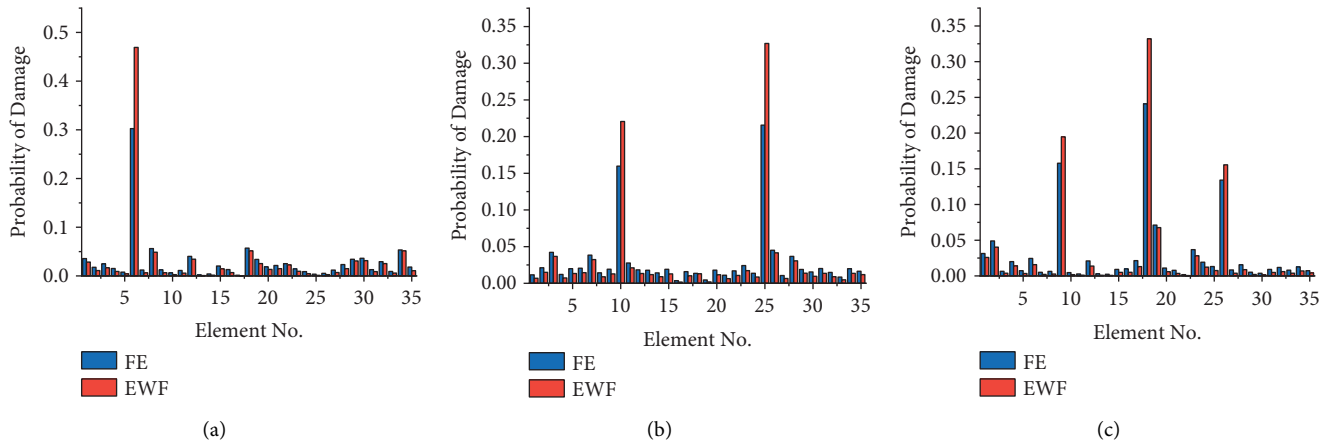

Figure 23: Damage identification results of forms 2, 3, and 4.

value is significantly higher than that of undamaged element. This shows that FE index and EWF index can accurately identify the preset single-point damage location.

It can be seen from Figure (b) that when there are two damage cases in the test beam, the FE index and the EWF index can also accurately identify the structural damage location. Comparing the peak value of the index at different damage locations, it can be seen that the location with the greater the damage degree has a higher peak value of the index and is easier to identify.

It can be seen from Figure (c) that when the structure is damaged at multiple points, the FE index and EWF index can still identify the damage location, but there is a more obvious mutation near the nondamaged position in the mid-span, as shown in the figure, and there is a mutation in Element 19, which interferes to a certain extent with the accurate judgment of the location of multipoint damage to structure. It can be seen from the figure that when the same degree of damage occurs in different positions of structure, the closer to the mid-span position, the stronger the sensitivity of the index, and the easier it is to be identified.

Comparing two-color histograms in the chart, it is found that peak values of EWF index (red) are obviously higher than those of FE index (blue). EWF values of mutation of undamaged points are smaller, meaning that EWF index has better antinoise ability and higher damage localization accuracy, which is consistent with simulation conclusion.

6. Conclusions

Based on the theory of modal strain energy, this paper adopts modal strain energy change (MSEC), modal strain energy ratio difference (MSERD), and cross-model modal strain energy change rate (RCMSEAM) as basic indexes to construct the fusion entropy (FE) index and entropy weight fusion (EWF) index by combining information entropy theory and Bayesian data fusion theory. The simulation examples of simply supported beam and truss structure are established, and damage localization, quantitative, and index antinoise analysis are carried out, respectively. Finally, the simply supported beam test is conducted to verify the results, and the following conclusions are drawn:

(1) In damage location analysis of simply supported beam, both FE index and EWF index can accurately identify the damage location. In truss structure, when the upper chord and the lower chord of truss structure are damaged, both indexes can effectively identify the damage location, while for web member damage, localization ability of the index needs to be improved. The effectiveness of FE index and EWF index in damage localization ability of actual structure is verified by simply supported beam test.

(2) In the analysis of damage degree, the damage degree functions of FE index and EWF index in simply supported beam and truss structure are obtained by polynomial fitting method. The RPE of the functional equation is kept within 2%, which is closer to the real damage than the literature [26], indicating that this method can effectively reflect the damage degree of the structure.

(3) In the antinoise analysis, FE index and EWF index can accurately identify the structural damage location under 10% noise, 15% noise, and test environment, showing good noise immunity and robustness.

(4) By comparison, EWF index is superior to FE index in damage localization, quantification, and antinoise analysis and can be preferred in practical operation. However, these two methods need to be further verified by field tests.

Data Availability

The data used to support the findings of this study are included within the article.

Conflicts of Interest

The authors declare that they have no conflicts of interest.

Acknowledgments

This work was supported by Natural Science Foundation of China (Grant no. 51868045), Natural Science Foundation of Anhui Province (Youth Foundation) (Grant no. 2008085QE247), Natural Science Foundation Provincial Key Projects in Anhui Province Universities (Grant no. KJ2019A0746), and Startup Fund for Doctor of Anhui Jianzhu University (Grant no. 2019QDZ08).

References

[1] G. Hui-yong and L. Zheng-liang, "Improvement and application of immune genetic algorithm in structural damage identification," *Journal of Civil, Architectural & Environmental Engineering*, vol. 34, no. 02, pp. 7–14, 2012.

[2] Z. Yu, D. Sheng-kui, and X. Chang-sheng, "Damage detection for simply supported bridge with bending stiffness fuzzy consideration," *Journal of Shanghai Jiaotong University*, vol. 23, no. 2, pp. 308–319, 2018.

[3] Y. X. Qin, B. L. Li, X. Li, and Y. Q. Z. Li, "Vibration analysis and control of nuclear power crane with MRFD," *International Journal of Applied Mechanics*, vol. 10, no. 08, p. 1850093, 2018.

[4] L. Peng, H. Min, and Z. Yang, "Real-time online automatic bridge modal identification," *Journal of Vibration, Measurement & Diagnosis*, vol. 2021, no. 01, pp. 76–84+201, 2021.

[5] J. P. Gu, Y. X. Qin, Y. Y. Xia, and Q. Q. H. B. Y. Y. H. Jiao, "Research on dynamic characteristics of composite towering structure," *International Journal of Applied Mechanics*, vol. 13, no. 08, 2021.

[6] W. Tong, T. Liang, and Z. Zhi-xiang, "Deflection curvature area difference method for damage location of bridge structures," *Advanced Engineering Sciences*, vol. 53, no. 06, pp. 165–174, 2021.

[7] Z. Bin, Z. Zhen, and Z. Qing-fang, "Multi-position damage identification and anti-noise analysis of cable-stayed arch-truss based on data fusion," *Journal of Building Structures*, vol. 41, no. S1, pp. 36–43, 2020.

[8] F. Xiao-ning, D. Chen-hui, and L. Zhi-hong, "Damage identification of the crane metal structures based on the wavelet transformation and modal curvature difference," *Journal of Safety and Environment*, vol. 21, no. 01, pp. 147–153, 2021.

[9] M. Jin-lei, Z. Zhong-liang, and W. Jian, "Identification method for crack damage of typical hull structures based on strain and vibration frequency," *Ship Engineering*, vol. 42, no. 05, pp. 46–50, 2020.

[10] N. Zi-sen, L. Don-gan, and C. Ming-zhi, "Structural damage identification based on frequency data and sparse regularization," *Acta Scientiarum Naturalium Universitatis Sunyatseni*, vol. 59, no. 06, pp. 148–153, 2020.

[11] Z. Guang, J. Xin, C. Ying, F. Zhi-wei, W. Ting-yue, and X. Zhi-liang, "Contact stiffness identification method based on modal strain energy," *Journal of Mechanical Engineering*, vol. 56, no. 9, p. 147, 2020.

[12] W. Xiao-shun, X. Ju-wei, and H. Yue-fang, "Damage localization of space trusses based on indicators expressed by cross-model modal strain energy," *Journal of Zhejiang University (Engineering Science)*, vol. 54, no. 02, pp. 248–256, 2020.

[13] H. Guan and V. M. Karbhari, "Improved damage detection method based on element modal strain damage index using sparse measurement," *Journal of Sound and Vibration*, vol. 309, no. 3-5, pp. 465–494, 2008.

[14] Z. Jin, P. Hua, and Y. Chun-hua, "Damage diagnosis of beam structures based on superimposed curvature modal change rate," *Engineering Mechanics*, vol. 29, no. 11, pp. 272–276, 2012.

[15] Z. Yi-nan, G. Mao-sheng, and Y. You, "A Review of Structural Damage Identification Methods," *World Earthquake Engineering*, vol. 36, no. 02, pp. 73–84, 2020.

[16] P. Cawley and R. D. Adams, "The location of defects in structures from measurements of natural frequencies," *The Journal of Strain Analysis for Engineering Design*, vol. 14, no. 2, pp. 49–57, 1979.

[17] H. Zi-chuan, M. Qi, and Z. Dan-fu, "Damage identification of L-shaped pipeline based on modal strain energy change rate," *China Civil Engineering Journal*, vol. 2020, no. S2, pp. 169–176, 2020.

[18] X. Zhi-peng, W. Shu-qing, X. Ming-qiang, and W. Hao-yu, "Structural damage identification based on TRIM," *Journal of Vibration and Shock*, vol. 2019, no. 17, pp. 251–259, 2019.

[19] N. Jie, W. Long-hua, and Z. Zhou-hong, "Damage identification method of beam type structures considering proportional damping," *Journal of Southeast University(Natural Science Edition)*, vol. 2018, no. 03, pp. 496–505, 2018.

[20] W. Xiao-shun, H. Chen-hui, and X. Ju-wei, "Damage site finding on space trusses by a virtual strain energy method," *Spatial Structures*, vol. 2020, no. 01, pp. 32–40, 2020.

[21] Y. Ting and Y. Fa-wen, "Evaluation of agricultural high quality development and diagnosis of obstacle factors based on entropy weight TOPSIS method," *Social Sciences in Yunnan*, vol. 2021, no. 05, pp. 76–83, 2021.

[22] L. Chen, "The evaluation of the quality of rural human settlements and its coordination with regional economy in China based on the production-living-ecological theory," *Chinese Journal of Agricultural Resources and Regional Planning*, vol. 105, p. 102278, 2020.

[23] L. Zhao-nan, H. Yao-kun, and L. Qi-jun, "Early warning evaluation and simulation analysis of resources and environmental carrying capacity in inland arid regions:an empirical analysis from ningxia," *Ecological Economy*, vol. 11, pp. 209–215, 2021.

[24] Y. Xing-cheng, W. Wu-yi, and Z. Yun-jia, "Spatial distribution and evolution characteristics of China's open economy development level," *Statistics & Decisions*, vol. 21, pp. 98–103, 2021.

[25] R. Yong-fen, Z. Qian, and Y. Ming, "Karst collapse risk assessment based on AHP-EWM-FT," *Journal of Safety and Environment*, vol. 49, p. 2017265, 2021.

[26] X. Chang-sheng, L. Ling-yun, and Z. Yu, "Damage identification of beam structures based on modal curvature utility information entropy," *Journal of Vibration and Shock*, vol. 17, pp. 234–244, 2020.

[27] N. Zhen-hua, Y. Wei-xing, and C. Liang-yan, "Bridge damage detection based on moving principal component analysis combining with transfer entropy," *Journal of Vibration Engineering*, vol. 05, pp. 1062–1072, 2020.

[28] A. A. Hidayat and B. Pardamean, "A bayesian-based approach for extracting the pion charge radius from electron-electron scattering data," *Chinese Physics C*, vol. 45, no. 8, p. 083101, 2021.

[29] K. Hemachandran, S. Tayal, P. M. George, P. Singla, and U. Kose, *Bayesian Reasoning and Gaussian Processes for Machine Learning Applications*, CRC Press, 2022.

[30] L. Hong-Lei, C. Shi, and Z. Jian-cang, "A bayesian data fusion algorithm for multi-source bouguer gravity anomalies and its application in the sichuan-yunnan region," *Chinese Journal of Geophysics*, vol. 09, pp. 3232–3245, 2021.

[31] L. Xue-yan and L. Li-chang, "Adoption of vibration response covariance and data fusion for damage identification," *Journal of Vibration Engineering*, vol. 2021, no. 01, pp. 141–149, 2021.

[32] B. Ji-gang, X. Shu-tao, and L. Xin-ji, *Information·Entropy·Economics :Road to Human Development*, Economic Science Pross, 2013.

[33] W. Ye-cheng, M. Jing, and J. Cong-jun, "Evaluation method on multi-stage Bayes information fusion for scatters HWIL simulation," *Journal of System Simulation*, vol. 07, pp. 1682–1688, 2021.

[34] S. Yu-pu, Z. Liang, and L. Zhi-xin, "Damage identification of space truss with incomplete measured data," *China Civil Engineering Journal*, vol. 1, pp. 10–15, 2009.

[35] F. Kun, Y. Yong-chun, and Z. Yi, "Damage detection method of a three-dimensional truss structure based on axial modal strain energy ratio," *Journal of Vibration and Shock*, vol. 12, pp. 169–173, 2013.

[36] Z. Hong, D. Zhong-dong, and O. Jin-ping, "Nolinear damage identification based on msvar modal," *Engineering Mechanics*, vol. 2021, no. 10, pp. 34–43, 2021.

[37] P. Juan, A. Sanchez, H. Seon Park, and H Adeli, "A novel methodology for modal parameters identification of large smart structures using MUSIC, empirical wavelet transform, and hilbert transform," *Engineering Structures*, vol. 147, pp. 148–159, 2017.

[38] Q. Shu-mao, Y. Hai-feng, W. Zi-yan, L. Meng-ying, and Y. Feng, "Damage identification of truss structure based on strain mode and sparse bayesian learning," *Chinese Journal of Computational Mechanics*, vol. 39, 2021.

[39] L. Heng-nuo, X. Tong, X. Shao-jun et al., "Structural damage detection of transverse guiding equipment of gear rack climbing type shiplift based on BP neural network," *Port & Waterway Engineering*, vol. 06, pp. 158–163, 2021.

[40] Z. Yu, D. Sheng-kui, X. Chang-sheng, L. Wan-run, and W. Li-xian, "Damage identification of simply supported bridge based on rotational angle influence lines method," *Transactions of Tianjin University*, vol. 24, no. 6, pp. 587–601, 2018.

[41] C. Hui and L. Xiu-ping, "Noise simulation in structural damage identification," *Journal of Vibration and Shock*, vol. 05, p. 106, 2010.